

Atomic Layer Deposition of Amorphous Niobium Carbide-Based Thin Film Superconductors

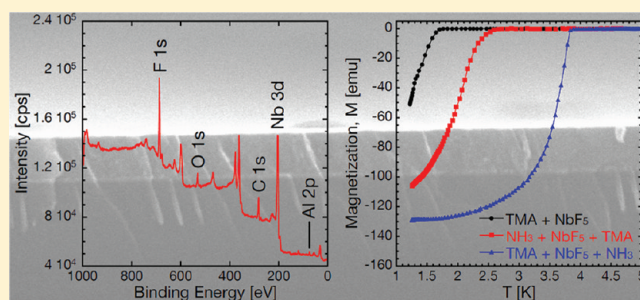
Jeffrey A. Klug,^{*,†} Thomas Proslir,^{†,‡} Jeffrey W. Elam,[§] Russell E. Cook,[†] Jon M. Hiller,[†] Helmut Claus,[†] Nicholas G. Becker,^{†,||} and Michael J. Pellin[†]

[†]Materials Science Division, [‡]High Energy Physics Division, and [§]Energy Systems Division, Argonne National Laboratory, 9700 South Cass Avenue, Argonne, Illinois 60439, United States

^{||}Department of Physics, Illinois Institute of Technology, 3101 South Dearborn Street, Chicago, Illinois 60616, United States

S Supporting Information

ABSTRACT: Niobium carbide thin films were synthesized by atomic layer deposition (ALD) using trimethylaluminum (TMA), NbF₅, and NbCl₅ precursors. In situ quartz crystal microbalance (QCM) measurements performed at 200 and 290 °C revealed controlled, linear deposition with a high growth rate of 5.7 and 4.5 Å/cycle, respectively. The chemical composition, growth rate, structure, and electronic properties of the films were studied over the deposition temperature range 125–350 °C. Varying amounts of impurities, including amorphous carbon (a-C), AlF₃, NbF_x, and NbCl_x, were found in all samples. A strong growth temperature dependence of film composition, growth rate, and room temperature DC resistivity was observed. Increasing film density, decreasing total impurity concentration, and decreasing resistivity were observed as a function of increasing deposition temperature for films grown with either NbF₅ or NbCl₅. Superconducting quantum interference device (SQUID) magnetometry measurements down to 1.2 K revealed a superconducting transition at $T_c = 1.8$ K in a 75 nm thick film grown at 350 °C with TMA and NbF₅. The superconducting critical temperature could be increased up to 3.8 K with additional use of NH₃ during ALD film growth.



INTRODUCTION

Early transition metal carbides are of interest in a wide variety of applications ranging from refractory coatings^{1,2} to catalysis.³ Thin amorphous films of transition metal carbides are of particular interest due to reduced brittleness and higher resistance to corrosion and laser damage in comparison to crystalline films.⁴ Niobium carbide is a refractory ceramic with a high melting point (3600 °C), excellent mechanical properties, and low electrical resistance (35 μΩ·cm).² Additionally, cubic NbC is a superconductor below 12 K.⁵ Thin films of NbC_x have been grown by a variety of techniques, including reactive^{6,7} and compound-target⁸ magnetron sputtering, cathodic arc deposition,⁹ and pulsed laser ablation.¹⁰ Atomic layer deposition (ALD)¹¹ is a synthesis technique wherein film growth is achieved by alternating exposure to two or more vaporous chemical precursors with each dose separated by an inert gas purge. Film growth proceeds in an atomic layer-by-layer fashion from sequential self-saturating chemical reactions between the precursor vapors and the solid film surface. ALD has been used previously to deposit a wide range of materials including metals, metal oxides, and metal nitrides. The atomic-layer control and excellent conformality characteristic of ALD has the potential to impact a variety of low-temperature superconductor-based devices and applications, including superconducting radiofrequency (SRF) resonator cavities used in high-energy particle

accelerators¹² and bolometers used for ultrasensitive radiation detection,¹³ which are currently limited by line-of-sight deposition techniques. However, there have been only two previously reported studies of superconductivity in ALD materials.^{14,15} Likewise, while considerable effort has been concentrated on the synthesis of transition metal nitride films by ALD for use as diffusion barriers in metal/semiconductor-based devices, there are comparably few examples of carbide film growth by atomic layer deposition. Elers et al. proposed in a 2002 patent the use of metal halides together with a boron-, silicon-, or phosphorus-containing carbon source (e.g., triethylborane) as route to ALD of numerous transition metal carbide films.¹⁶ However, to date, published reports of transition metal carbide ALD have examined the synthesis of a limited selection of materials: tungsten carbide (WC_x),¹⁷ tungsten carbo-nitride (WN_xC_y),¹⁸ and tantalum carbo-nitride (TaN_xC_y).^{19–21}

We previously reported the use of niobium pentafluoride (NbF₅) as a precursor for ALD of niobium silicide (NbSi) using disilane (Si₂H₆) and niobium oxide (Nb₂O₅) using either H₂O or H₂O₂.¹⁵ Here, we demonstrate the ALD of superconducting

Received: August 8, 2011

Revised: November 1, 2011

Published: November 28, 2011

NbC_x using NbF₅ or NbCl₅ together with trimethylaluminum (TMA) [Al(CH₃)₃] as both a carbon source and a reducing agent. TMA is widely used as a precursor in aluminum oxide (Al₂O₃) ALD. However, TMA can also function as a reducing agent in the ALD of metal nitrides using halide precursors and ammonia.^{22–24} ALD of both Ti(Al)N²² and Ta(Al)N^{23,24} have been previously reported using TMA together with ammonia and metal chloride-based precursors. In a 2007 patent Härkönen and co-workers described an ALD-like process for depositing transition metal and carbon-containing films using metal halides (e.g., TiCl₄) and an organometallic carbon source (TMA) at temperatures between 250 and 550 °C.²⁵ However, while the Härkönen work employed an alternating pulse–purge deposition mode, no claim or investigation was made as to whether the growth process was self-limiting. Furthermore, the experimental examples presented by Härkönen largely concern depositions performed above the thermal decomposition temperature of TMA (~330 °C).^{26,27} In contrast, the present work has been confined to growth temperatures below 350 °C with in situ measurements performed to examine the self-limiting nature of the ALD reactions. To our knowledge, this is the first reported study of a self-saturating ALD process which relies on TMA as the sole reducing agent.

EXPERIMENTAL METHODS

All ALD experiments were carried out in a custom viscous-flow reactor²⁸ in which the deposition zone was comprised of a 5 cm diameter Inconel 600 flow tube. Reactor temperature was maintained between 60 and 500 °C by an external three-zone computer-controlled resistive heater system. The reactor temperature was measured using type-K thermocouples located at nine spots along the length of the flow tube to verify uniformity. A constant flow of ultrahigh-purity nitrogen (UHP, 99.999%, Airgas) at ~360 sccm with a pressure of ~1.3 Torr was maintained by mass flow controllers. An inert gas purifier (Entegris GateKeeper, part no. CE70KFI4R) was used to further purify the nitrogen gas by reducing the contamination level of H₂, CO, and CO₂ to less than 1 ppb and O₂ and H₂O to less than 100 ppt. During the in situ quartz crystal microbalance (QCM) studies the reactor was equipped with a modified Mextek BSH-150 bakeable sensor head loaded with an unpolished AT-cut quartz crystal sensor (Tangidyne/VB) and interfaced to a computer via a Mextek TM400 film thickness monitor.

Niobium carbide ALD films were grown using alternating exposures to TMA (97%, Sigma-Aldrich) and either NbF₅ (98%, Sigma-Aldrich) or NbCl₅ (anhydrous, 99.995%, Sigma-Aldrich). The solid NbF₅ and NbCl₅ precursors were held in stainless steel bubblers at 65 and 115 °C, respectively. The NbCl₅ bubbler was lined with a quartz insert to reduce etching of the stainless steel. Niobium carbo-nitride films were grown with the additional use of NH₃ (anhydrous, 99.9995%, Sigma-Aldrich).

For ex situ studies, films were deposited at temperatures between 100 and 350 °C on Si(001) (*p*-type (boron), 10–20 μΩ·cm, MEMC Electronic Materials, Inc.), and fused quartz (ground and polished G.E. 124 fused quartz, Technical Glass Products, Inc.) substrates. All substrates were 1–2 cm in size. Film composition, thickness, morphology, and structure were characterized by X-ray photoemission spectroscopy (XPS), Rutherford backscattering spectroscopy (RBS), X-ray reflectivity (XRR), atomic force microscopy (AFM), scanning electron microscopy (SEM), transmission electron microscopy (TEM), and X-ray diffraction (XRD).

Chemical composition was analyzed using XPS spectra collected with a 100 mm mean radius hemispherical energy analyzer (VSW HA-100) and Mg Kα radiation (1253.6 eV) from a dual-anode X-ray source (Perkin-Elmer PHI 04-500) operated at 300 W/15 kV. The XPS chamber was equipped with an ion gun (Perkin-Elmer PHI 04-303) which allowed for Ar ion milling to remove surface contamination. For all samples, XPS measurements were made following a 5–10 min Ar ion-milling step using an ion beam voltage of 5 kV, an emission current of 20 mA, and an Ar pressure of 10 mPa. Elemental concentrations were determined from survey scans using an analyzer pass energy of 44 eV. Chemical compositions were obtained from higher resolution scans using a 22 eV analyzer pass energy. XPS spectra were charge corrected (for insulating samples) and adjusted to account for the spectrometer work function (~2 eV) by setting the binding energy of the adventitious (C–C, C–H) carbon 1s peak equal to 284.8 eV. In order to independently verify the accuracy of the XPS analysis, RBS measurements (Evans Analytical Group, Sunnyvale, CA) were performed on several samples using a 2.275 MeV He²⁺ ion beam incident along the sample normal. Backscattered He⁺⁺ ions were measured at detector angles of 160°, ~97°, and 107° to characterize the density and bulk (nonsurface) elemental composition of films deposited at 150, 250, and 350 °C.

XRR measurements were made with a Philips X'Pert Pro MRD diffractometer using Cu Kα radiation and operated at 30 kV/40 mA. Surface roughness was measured using a Veeco NanoScope V multimode AFM using a silicon tip and operating in tapping mode with a 1 μm × 1 μm scan size. Secondary electron images were acquired using a Hitachi S4700 field emission SEM. Convergent beam electron diffraction (CBED) and cross-sectional TEM were performed with a FEI CM30T TEM. XRD measurements were made with a Rigaku Miniflex⁺ desktop X-ray powder diffractometer equipped with a Cu tube and operated at 30 kV/15 mA.

Electrical properties were characterized at room temperature by four-point probe (Lucas Signatone S-301-6 probe stand with a Keithley 224 programmable current source) and Hall effect (Ecopia HMS-3000 Van de Pauw system) measurements. Superconducting properties were studied by superconducting quantum interference device (SQUID) magnetometry using a custom-built instrument operated down to 1.2 K under an external magnetic field of 10 mGauss.

RESULTS AND DISCUSSION

In Situ Studies. The in situ QCM studies showed linear growth at 200 and 290 °C for alternating exposures to TMA and NbF₅. Figure 1 shows the results obtained at 200 °C using a TMA/NbF₅ timing sequence (TMA exposure–purge–NbF₅ exposure–purge) of (1–10–2–10) where all times are given in seconds. The film growth initiated immediately on an Al₂O₃ surface and reached a constant growth rate after 10–15 cycles. An abrupt mass increase was observed during the NbF₅ exposures followed by a slower apparent decrease in mass over the 10 s purge to a steady value of 292 ng/cm². The QCM is sensitive to changes in both mass and temperature,²⁹ and even small temperature perturbations resulting from changes in gas flow during introduction and removal of reactants can result in significant apparent mass changes. The QCM pulse shape for the NbF₅ dose/purge here is similar to that observed in the NbSi ALD process,¹⁵ and the apparent mass loss during the NbF₅

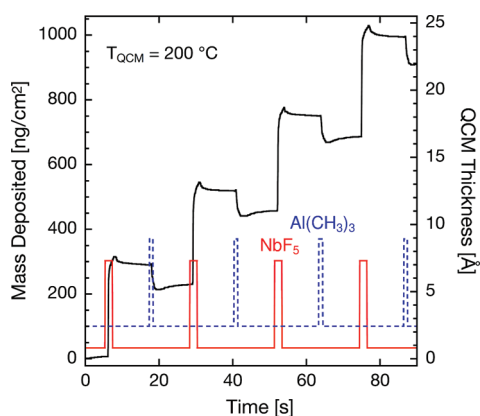


Figure 1. QCM-measured film thickness vs time during alternating TMA/NbF₅ exposures at 200 °C. The timing sequence was (1–10–2–10). Thickness was calculated assuming a film density of 4.17 g/cm³ (as measured by XRR).

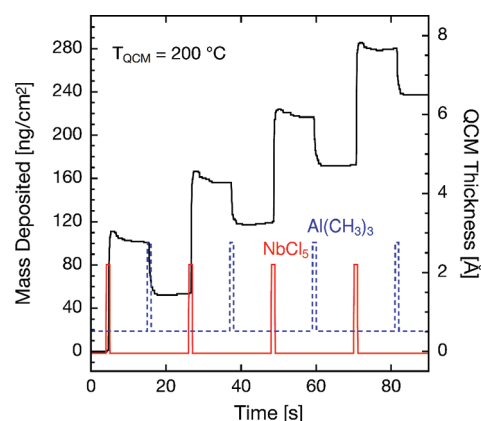


Figure 3. QCM-measured film thickness vs time during alternating TMA/NbCl₅ exposures at 200 °C. The timing sequence was (1–10–1–10). Thickness was calculated assuming a film density of 3.65 g/cm³ (as measured by XRR).

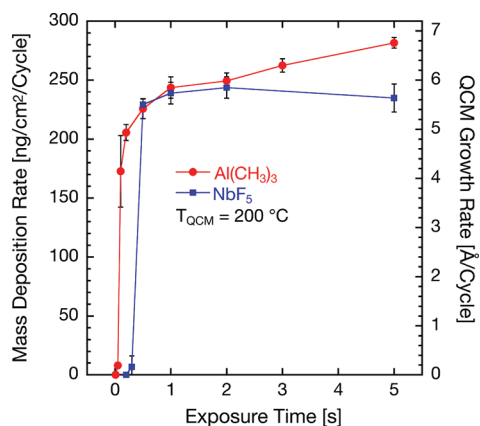


Figure 2. Mass deposition and QCM thickness vs TMA (circles) and NbF₅ (squares) exposure time at 200 °C. Two second NbF₅ exposures were used during the TMA measurement, 1 s TMA exposures were used during the NbF₅ measurement, and 10 s N₂ purges were used following each precursor exposure in both cases.

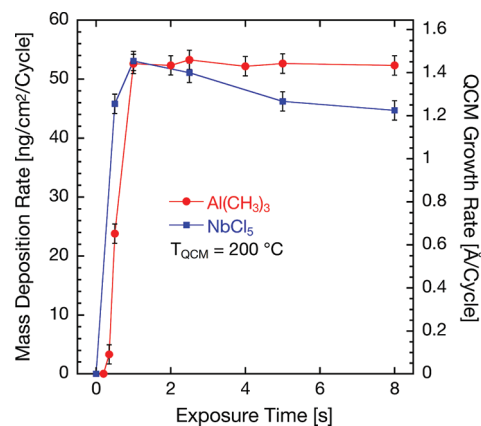


Figure 4. Mass deposition vs TMA (squares) and NbCl₅ (circles) exposure time at 200 °C. One second NbCl₅ exposures were used during the TMA measurement, 1 s TMA exposures were used during the NbCl₅ measurement, and 10 s N₂ purges were used following each precursor exposure in both cases.

purge is attributed to a slow relaxation of the QCM surface temperature back to thermal equilibrium following the NbF₅ exposure. An abrupt mass decrease occurs during the TMA exposures followed by a slow apparent mass gain during the 10 s purge. A growth rate of 5.7 Å/cycle was calculated assuming a film density of 4.17 g/cm³ (as measured by XRR). An identical growth rate was measured by XRR. Similar results were obtained at 290 °C with a growth rate of 4.3 Å/cycle calculated assuming a density of 4.51 g/cm³ (not shown).

Figure 2 shows the dependence of the deposition rate upon precursor exposure times as measured by QCM at 200 °C. Pulse sequences of ($x-10-2-10$) and ($1-10-x-10$) were used during the TMA and NbF₅ measurements, respectively. The mass deposition rates shown represent the average of 3–6 separate ALD cycles, and the film growth rate was calculated assuming a density of 4.17 g/cm³ as in Figure 1. The deposition rate was found to increase rapidly for increasing exposure times for either precursor of less than 0.5 s. While measurable film growth was observed for TMA doses as short as 0.05 s, the NbF₅ dose results show a small delay time (~ 0.5 s) that we attribute to complete consumption of the NbF₅ precursor on the walls of the

flow tube upstream of the QCM in our traveling wave reactor. The mass deposition rate rises to 240 ng/cm²/cycle as each exposure approaches 1 s and remains constant between 1 and 2 s. This demonstrates the self-limiting behavior of each reaction. For TMA exposure times exceeding 2 s the growth rate increases at a rate ~ 11 ng/cm²/s and reaches 280 ng/cm² for 5 s exposures. The origin of this behavior is unknown, but similar phenomena have been observed previously in QCM measurements of Al₂O₃ ALD using TMA and H₂O.^{28,30}

Linear, controlled growth at 200 °C was also observed when NbF₅ was replaced by NbCl₅, as shown in Figures 3 and 4. Figure 3 shows the QCM results obtained at 200 °C using a TMA/NbCl₅ pulse sequence of 1–10–1–10. As with NbF₅, growth initiated immediately on an Al₂O₃ surface and the overall QCM pulse shapes are qualitatively similar to those of the NbF₅ process. However, compared to the NbF₅ QCM trace a larger mass decrease during the TMA dose is observed relative to the mass increase accompanying the NbCl₅ dose. This is likely due to the relative weights of the chlorine and fluorine ligands removed during the TMA pulse in each respective ALD process. A significantly

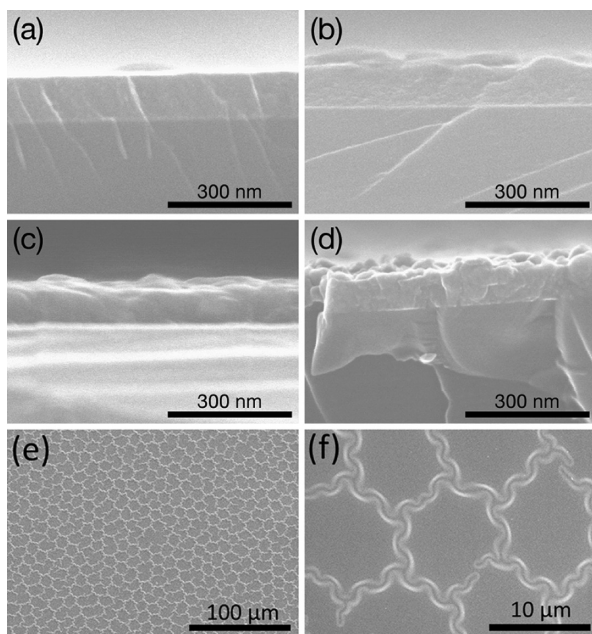


Figure 5. SEM cross-sections of films grown with TMA/NbF₅ on Si(001) at (a) 200, (b) 250, (c) 300, and (d) 350 °C show an increase in roughness with higher deposition temperature. Plan-view SEM images (e and f) at different magnification show the surface of degraded TMA/NbCl₅ ALD films grown at 300 °C and exposed to air for ~5 weeks. All films were deposited with 200 ALD cycles using a timing sequence of 1–5–1–5.

smaller growth rate of 1.4 Å/cycle was estimated for the TMA/NbCl₅ synthesis assuming a film density of 3.65 g/cm³. The film density used here was measured by XRR for a film deposited at 250 °C as films grown at 200 °C were not stable in air for more than a few hours. Films grown at 200 °C changed from a smooth coating to powder within hours of air exposure, which we attribute to hydrolysis of unreacted or partially reacted NbCl₅ incorporated in the films.

Figure 4 shows the dependence of the deposition rate upon TMA and NbCl₅ precursor exposure times as measured by QCM. Pulse sequences of (*x*–10–1–10) and (1–10–*x*–10) were used for the TMA and NbCl₅ saturation measurements, respectively. The mass deposition rates shown represent the average of 3–6 separate ALD cycles, and the film growth rate was calculated assuming a density of 3.65 g/cm³ as in Figure 3. The deposition rate was found to increase rapidly for increasing exposure times for either precursor of greater than 0.5 s. The mass deposition rate rises to 53 ng/cm²/cycle as each exposure approaches 1 s and remains roughly constant between 1 and 2 s, thereby demonstrating the self-limiting behavior of each reaction. While the growth rate remains constant for TMA doses as long as 8 s, increasing NbCl₅ exposure times lead to a decreasing deposition rate: from 51 ng/cm²/cycle for 2.5 s doses to 45 ng/cm²/cycle for 8 s doses. The decrease in growth rate observed for NbCl₅ exposures longer than 2 s suggests that the chloride precursor etches the growing film. Previous studies have reported similar behavior in ALD growth of nitrides and oxides using metal chloride precursors.^{31,32} To minimize this effect, short NbCl₅ doses (1 s) were used for subsequent film growth.

Ex Situ Studies. All films grown from TMA and NbF₅ at or above 125 °C were stable in air, dark in color, and optically

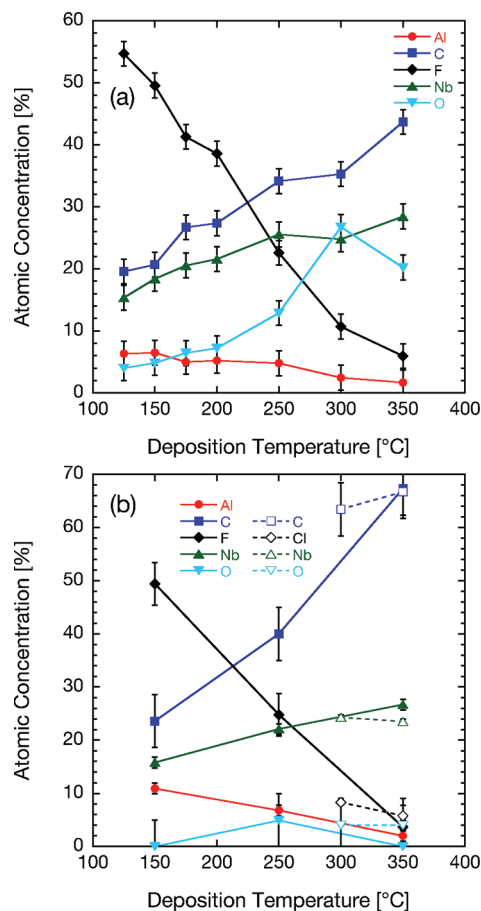


Figure 6. Film composition measured by (a) XPS and (b) RBS vs deposition temperature between 125 and 350 °C. XPS spectra were acquired following a 5–10 min Ar ion-milling step to remove surface contamination. Data from films grown with NbF₅ and NbCl₅ are represented by filled and open shapes, respectively.

reflective (mirror-like). Those deposited below 200 °C were blue in color with a gradual darkening as the growth temperature approached 200 °C. Films grown at 200 °C and above were metallic with a dark gray color, while those grown at 100 °C were bright blue upon removal from the reactor but changed to a cloudy silver color within a few hours of exposure to air. Due to the higher vaporization temperature of NbCl₅ compared to NbF₅ no films were grown from TMA and NbCl₅ below 200 °C. All NbCl₅ samples appeared metallic and brownish-gray in color upon removal from the reactor. As discussed in the previous section, films grown at 200 °C changed from a smooth coating to powder within hours of air exposure. Those grown at 250 and 300 °C were stable in air for a longer period of time of 2–5 weeks. SEM images of the powder-like surface revealed surprising self-organized patterns with a honeycomb symmetry, as can be seen in Figure 5e and 5f. The white serpentine structures are likely to be more insulating (oxygen rich) than the rest of the film, although EDAX revealed no compositional differences probably due to the fact that the EDX sampling width is on the order of the structure itself ~7 μm. Long-range interactions such as elastic constraints developed upon oxidation are known to create such structures in similar systems.³³ Only the films grown at 350 °C were stable in air indefinitely. Consequently, only films grown from TMA and NbF₅ at or above a substrate temperature of

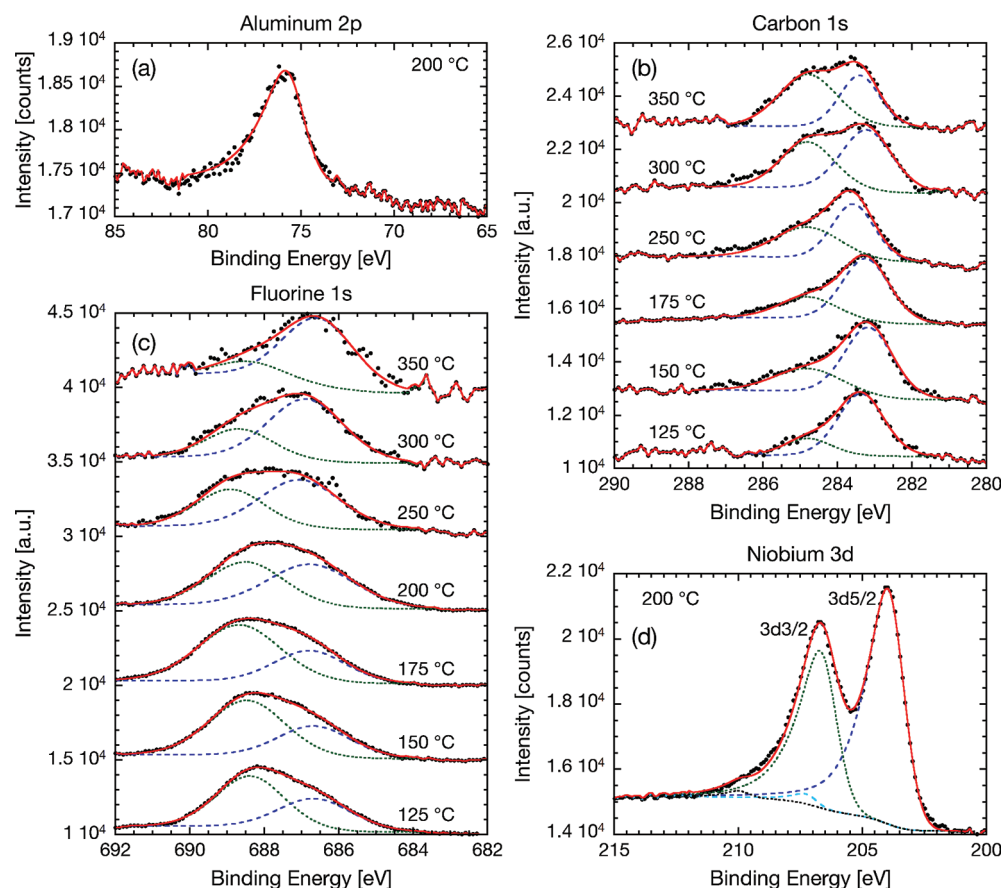


Figure 7. XPS peak analysis for (a) aluminum 2p, (b) carbon 1s, (c) fluorine 1s, and (d) niobium 3d in films grown with TMA and NbF_5 . The intensities in b and c are normalized and displaced vertically for clarity. Aluminum 2p peak was fit with a single asymmetric Gaussian–Lorentzian (GL) mixture centered at 76.2 eV. The carbon 1s peak was fit with two symmetric GL mixtures centered at 283.3 and 284.8 eV. The fluorine 1s peak was fit with two symmetric GL mixtures centered at 686.8 and 688.6 eV. The niobium 3d peaks were fit with two pairs of asymmetric GL mixtures, with the two 3d_{5/2} peaks centered at 204.0 and 207.3 eV.

125 °C and TMA and NbCl_5 at or above a substrate temperature of 250 °C were characterized further.

XPS and RBS Measurements. All films deposited from TMA and NbF_5 were found to contain aluminum, carbon, fluorine, niobium, and oxygen, and the relative concentrations of each were found to depend on the deposition temperature (Figure 6). The results of the XPS survey analysis are shown in Figure 6a. According to XPS, the aluminum content decreased steadily from 6 atom % at 125 °C to 2 atom % at 350 °C. The fluorine content decreased much more dramatically from 55 atom % at 125 °C to 6 atom % at 350 °C. In contrast, the carbon and niobium content both increased with deposition temperature, with carbon increasing from 20 atom % at 125 °C to 44 atom % at 350 °C and niobium increasing from 15 atom % at 125 °C to 28 atom % at 350 °C. The oxygen content appeared to increase with higher growth temperature up to maximum of 27 atom % at 300 °C before decreasing to 20 atom % at 350 °C. However, as shown in Figure 6b, the RBS measurements found no significant levels of oxygen in the film bulk. No oxygen was detected in the films grown at 150 or 350 °C, while 4.9 atom % was found in the 250 °C film. The estimated uncertainty of the RBS measurement of oxygen concentration was ± 5 atom %. This indicates that the oxygen observed by XPS was most likely due to incomplete removal of the surface oxide layer produced by exposure to air after deposition.

Despite these differences, the XPS and RBS showed similar trends in the aluminum, carbon, fluorine, and niobium concentrations versus the deposition temperature. Furthermore, if the XPS concentrations are adjusted to account for surface oxides which are not present in the bulk film, the two measurements are quantitatively similar. For example, 20 atom % of the film grown at 350 °C was found by XPS to be oxygen, which suggests a total of 28–30 atom % of the XPS analyzed volume was niobium oxide (NbO_2 or Nb_2O_5). Correcting for this, the remaining film would be 2.4 atom % aluminum, 61–63 atom % carbon, 8.3–8.6 atom % fluorine, and 26–28 atom % niobium, all of which are, within experimental error, equal to the atomic concentrations determined by RBS.

Detailed XPS analysis (22 eV pass energy) of the aluminum 2p, carbon 1s, fluorine 1s, and niobium 3d peaks is shown in Figure 7a, 7b, 7c, and 7d, respectively. Peak fitting was performed with the CasaXPS software package.³⁴ The aluminum 2p binding energy was 76.2 eV, which is within 0.1 eV from the value reported for AlF_3 (76.3 eV).³⁵ Two carbon 1s peaks were observed with binding energies 283.3 eV (C_1) and 284.8 eV (C_2), which are close to those reported for NbC (281.9 eV)³⁶ and elemental carbon.³⁷ The fluorine 1s peak was fit with two peaks centered at 686.8 (F_1) and 688.6 eV (F_2). The lower energy peak F_1 corresponds closely to the binding energy reported for $\text{AlF}_3 \cdot 3\text{H}_2\text{O}$ (686.3 eV).³⁸ The higher energy peak

Table 1. Estimated TMA/NbF₅ Film Composition Calculated from Oxide-Corrected XPS Data^a

deposition temperature [°C]	NbC [atom %]	NbF _x [atom %]	AlF ₃ [atom %]	a-C [atom %]
125	31(3)	35(2)	29(3)	5.0(5)
250	37(3)	23(2)	17(3)	23(1)
350	45(2)	9(1)	9(4)	37(1)

^a Parenthetical values represent uncertainty accounting for both the uncertainty of the XPS atomic compositions and the range of probable stoichiometries of the niobium oxides and fluorides represented in the XPS spectra. Regarding notation, 5.0(5) represents 5.0 ± 0.5 .

Table 2. Estimated TMA/NbCl₅ Film Composition Calculated from RBS Data^b

deposition temperature [°C]	NbC [atom %]	NbCl _x [atom %]	a-C [atom %]
300	44(1)	11(1)	41(1)
350	44(1)	7(1)	45(1)

^b The 4 atom % oxygen concentration detected by RBS was not subtracted; otherwise, the film was assumed to contain only NbC, NbCl_x ($3 \leq x \leq 5$), and a-C. Parenthetical values represent uncertainty accounting for the range of probable stoichiometries of the niobium chlorides represented in the data.

F₂ is consistent with a metal fluoride with the metal ion in an oxidation state greater than 3.³⁷ The niobium 3d peaks were fit with four peaks corresponding to two distinct pairs of 3d_{3/2} and 3d_{5/2} states. The binding energy of the larger (Nb₁) Nb 3d_{5/2} peak was 204.0 eV, which is close to the value reported for NbC (203.7 eV).³⁹ The binding energy of the smaller (Nb₂) Nb 3d_{5/2} peak was 207.3 eV, which is slightly less than that reported for NbF₅ (209.6 eV)³⁵ and consistent with a reduced niobium fluoride NbF_x ($x < 5$) since the Nb 3d binding energies would shift to lower values for decreasing oxidation number.⁴⁰ The smaller Nb 3d_{5/2} binding energy is also within the range expected for niobium oxide,³⁷ which suggests that some portion of the Nb₂ signal can likely be attributed to surface oxide in samples where a significant oxygen concentration was detected.

Table 1 shows the estimated TMA/NbF₅ film composition calculated from the oxide-corrected XPS data for films grown at 125, 250, and 350 °C. The NbC content increased with deposition temperature from approximately 31 atom % at 125 °C to 45 atom % at 350 °C. The amount of partially reacted or unreacted NbF_x in the films decreased sharply from 35 atom % at 125 °C to 9 atom % at 350 °C, and the AlF₃ content likewise decreased from 29 atom % at 125 °C to 9 atom % at 350 °C. The decrease in AlF₃ is likely due to a change in the favorability of AlF₃ formation with increasing growth temperature, rather than temperature-activated volatility of the highly stable AlF₃ (mp 1290 °C), that is, formation of an alternate volatile aluminum compound (e.g., Al(CH₃)₂F₂) is likely preferred at higher temperatures. The carbon content was found to increase significantly with increasing growth temperature, from 5 atom % at 125 °C to a surprisingly high 37 atom % at 350 °C. The mechanism responsible for such a high carbon concentration is unclear at present, although additional characterization (e.g., infrared spectroscopy) looking for a comparably high hydrogen content might provide some insight. Additional details and discussion of the XPS analysis are provided in the Supporting Information.

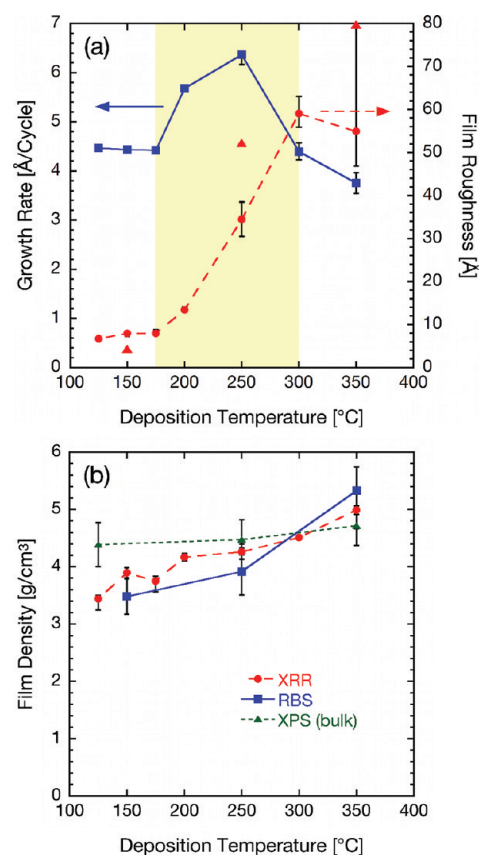


Figure 8. Deposition temperature dependence of TMA/NbF₅: (a) film growth rate determined by XRR (squares) and roughness determined by XRR (circles) and AFM (triangles) and (b) film density determined by XRR (circles) and RBS (squares) and calculated (triangles) from bulk densities (NbC, NbF_x, AlF₃, and a-C) and XPS chemical composition.

Compositional analysis of films grown with NbCl₅ included only RBS measurements of samples deposited at 300 and 350 °C, the results of which are plotted in Figure 6b. The 300 °C film was found to contain 24.3 atom % niobium, 8.3 atom % chlorine, 63.4 atom % carbon, and 4 atom % oxygen. The 350 °C film was found to contain 23.5 atom % niobium, 5.8 atom % chlorine, 66.7 atom % carbon, and 4 atom % oxygen. In both films the oxygen concentration was less than the uncertainty of the RBS measurement of oxygen (± 5 atom %), indicating negligible oxygen contamination. Notably absent from either film is aluminum, which we attribute to the greater volatility of AlCl₃ (mp 192.6 °C) compared to AlF₃ (1290 °C). The absence of aluminum also suggests that the chlorine content in both films is due to the presence of niobium chloride, the total concentration of which is similar to the niobium fluoride which remains in the NbF₅ films. The 5.8 atom % chlorine measured in the 350 °C sample signals that approximately 1.2–1.9 atom % of the film is niobium bound to chlorine implying that 7.0–7.7 atom % of the film is composed of NbCl_x. If this is subtracted from the total niobium concentration, then approximately 43.2–44.6 atom % of the film is NbC (assuming a 1:1 stoichiometry) and 44.4–45.1 atom % of the film is amorphous carbon (assuming the same chemical species observed in the films grown with NbF₅). This suggests a slightly more carbon-rich film compared to the NbF₅ sample grown at the same temperature (Table 1). An estimated composition calculated for the 300 °C film is listed in Table 2.

XRR, SEM, and XRD Measurements. The effect of deposition temperature on film growth rate, density, and roughness was evaluated using XRR measurements of films grown between 125 and 350 °C. Figure 8 shows the results of the XRR analysis of films grown with NbF₅. The growth rate (Figure 8a) was roughly constant (~4.5 Å/cycle) up to a deposition temperature of 175 °C. However, at higher temperatures the growth rate at first increased up to a maximum of 6.3 Å/cycle at 250 °C and subsequently decreased for temperatures above 250 °C: 4.5 Å/cycle at 300 °C and 3.8 Å/cycle at 350 °C. The nonmonotonic variation of the growth rate as a function of growth temperature is somewhat surprising, and the exact cause of this behavior is unknown. Possible explanations include a temperature-dependent variation in the surface species involved in film growth or a change in the density of active surface sites for one or both precursors. Alternatively, while the QCM results obtained at 200 and 290 °C suggest linear, controlled growth, it is not known whether film growth can appropriately be described as ALD throughout the entire temperature range examined. Films grown above 350 °C (not shown) showed evidence of uncontrolled growth, likely due to thermal decomposition of the TMA precursor. For films grown with NbCl₅ (not shown), XRR measurements revealed a linear increase in growth rate with increasing temperature in the process window examined: from 1.9 Å/cycle at 250 °C to 2.2 Å/cycle at 300 °C and to 2.5 Å/cycle at 350 °C. This seems to contradict the etching behavior inferred from the NbCl₅ QCM data since etching is expected to accelerate with increasing substrate temperature, leading to a decreasing growth rate.³² However, this effect can be minimized with the use of appropriately small precursor doses.⁴¹ While the use of short NbCl₅ doses cannot alone account for the increasing growth rate, if the effect of etching is minimized and an alternate temperature dependence (e.g., variation in surface species or active sites) dominates a net increasing trend may result.

Figure 8b shows the deposition temperature dependence of the measured density of films grown with NbF₅. For all growth temperatures film densities much lower than that of bulk NbC (7.82 g/cm³) were observed by XRR and RBS. Both measurements showed density increasing with deposition temperature, from 3.44 g/cm³ at 125 °C to 4.99 g/cm³ at 350 °C. The uniformly low densities were attributed to the high impurity content. The change in film density can be understood in part as a reflection of the temperature-dependent film composition. To illustrate this effect, estimated film densities were calculated from bulk values for NbC (7.82 g/cm³), AlF₃ (3.1 g/cm³), NbF₅ (2.7 g/cm³), NbF₄ (4.0 g/cm³), NbF₃ (4.2 g/cm³), and a-C (1.8–2.1 g/cm³). The bulk densities were weighted using oxide-corrected chemical concentrations determined by XPS for films grown at 125, 250, and 350 °C (Table 1). The weighted average bulk density values, shown in Figure 8b, reveal a temperature trend similar to the XRR- and RBS-determined densities with the best agreement at 350 °C and the poorest agreement at 125 °C. It is possible that incomplete reactions at low temperatures lead incorporation of hydrogen, which was not measured in this study.³⁰ Alternatively, the films might be porous. XRR measurements of films grown with NbCl₅ between 250 and 350 °C (not shown) showed lower densities (3.65–4.25 g/cm³) than those of films grown with NbF₅. However, a similar positive dependence on deposition temperature was observed.

The effect of growth temperature on the XRR-determined surface roughness of films grown with NbF₅ is shown in Figure 8a. Films grown below 200 °C were smooth, with an approximately

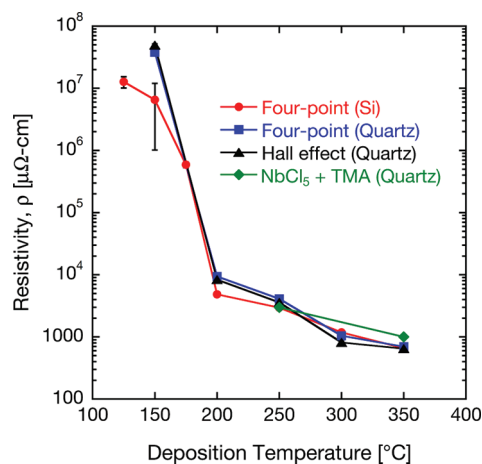


Figure 9. Room-temperature resistivity versus deposition temperature. Resistivity was measured by four-point probe for films grown with NbCl₅ on fused quartz (diamonds), films grown with NbF₅ on Si(001) (circles), and fused quartz (squares) and by Hall effect measurement for films grown with NbF₅ on fused quartz (triangles).

constant roughness of less than 0.8 nm. However, a dramatic increase in surface roughness was observed for films grown above 175 °C: from 1.3 nm at 200 °C to 5.9 nm at 300 °C. For significantly roughened surfaces the Gaussian surface roughness assumed in the XRR analysis is generally not appropriate and can underestimate the true root-mean-square (rms) roughness.⁴² Accordingly, surface roughness was also measured by AFM for samples grown at 150, 250, and 350 °C (Figure 8a) for comparison. For the 150 °C film, the AFM rms roughness was 0.4 nm, comparable to that measured by XRR. However, for the 250 and 350 °C films which each have a higher roughness, the AFM rms values were 5.2 and 8.0 nm, respectively. A similar result was observed via cross-section SEM with a clear roughening visible with increasing growth temperature. Figure 5a, 5b, 5c, and 5d shows SEM images of films prepared on Si(001) using 200 cycles of TMA/NbF₅ at 200, 250, 300, and 350 °C, respectively. The observed increase in surface roughness with growth temperature resembles an amorphous to crystalline transition where the roughness results from preferred growth along certain crystalline planes. However, films grown on Si(001) and fused quartz between 150 and 350 °C appeared amorphous by XRD, with no features observed corresponding to crystalline NbC_x or AlF₃. This finding can be attributed to the relatively large concentration of impurities which are expected to disrupt the crystal lattice and thereby stabilize an amorphous or nanocrystalline alloy.⁴³ To investigate the film structure further, samples grown at 200 and 350 °C were characterized by electron diffraction and cross-sectional imaging via TEM (Supporting Information). Both films were observed to contain mixtures of amorphous and nanocrystalline regions, with the bottom 60–70 nm of both ~100 nm thick films amorphous as confirmed by CBED. In the crystalline regions, the crystallite diameter ranges from ~1–5 nm.

Films grown with NbCl₅ were comparably smooth throughout the temperature regime examined. Furthermore, the XRR analysis of the NbCl₅ samples showed a slightly decreasing roughness with increasing deposition temperature: from 1.1 nm at 250 °C to 0.8 nm at 350 °C. This implies that no amorphous to (nano)crystalline transition occurs in this temperature range.

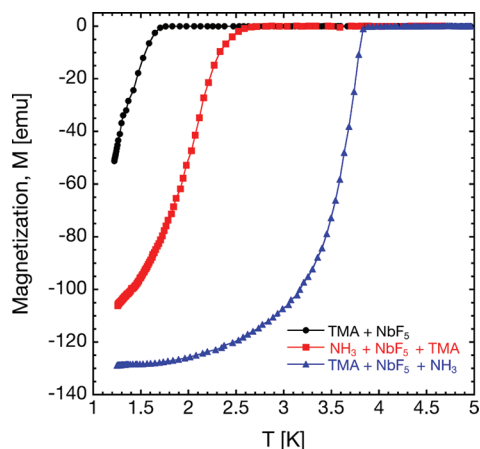


Figure 10. SQUID measurements of superconducting critical temperature T_c for films grown on Si(001) with the precursor sequence TMA + NbF₅ (circles), NH₃ + NbF₅ + TMA (squares), and TMA + NbF₅ + NH₃ (triangles).

No diffraction peaks were observed from TMA/NbCl₅ films deposited on fused quartz.

Electrical Properties. The electrical properties of films grown with either NbF₅ or NbCl₅ were strongly influenced by deposition temperature. In each case a lower resistivity was measured for films grown at higher temperatures, which is consistent with the higher observed film densities and overall lower total impurity levels. Figure 9 shows the effect of deposition temperature on the room-temperature DC resistivity measured for a series of 200 cycle TMA/NbF₅ and TMA/NbCl₅ films. The resistivity values extracted from both four-point probe and Hall effect measurement decrease approximately exponentially as a function of growth temperature with two distinct slopes. The TMA/NbF₅ film resistivity decreased from $4.0 \times 10^7 \mu\Omega \cdot \text{cm}$ at 150 °C to $9.4 \times 10^3 \mu\Omega \cdot \text{cm}$ at 200 °C and to $700 \mu\Omega \cdot \text{cm}$ at 350 °C. The change in slope observed at 200 °C in the resistivity data suggests two separate regimes: a high-resistivity (HR) regime and a low-resistivity (LR) regime. This can be attributed to a combined effect of the increasing concentration of conductive NbC and the changing composition of the impurities. At low growth temperatures, the dominant impurities are insulating fluorides (NbF_x and AlF₃) which lead to a high film resistivity. The amorphous carbon which dominates the impurity content at higher temperatures leads to a lower film resistivity. Four-point probe measurements of TMA/NbCl₅ films found that the room-temperature resistivity decreased from $3.0 \times 10^3 \mu\Omega \cdot \text{cm}$ at 250 °C to $1.0 \times 10^3 \mu\Omega \cdot \text{cm}$ at 350 °C.

Results from SQUID measurements of films grown with NbF₅ are shown in Figure 10. Only films deposited at or above 350 °C exhibited a superconducting transition above 1.2 K, with a transition observed at $T_c = 1.8$ K in a 75 nm thick film grown at 350 °C with 200 cycles of TMA and NbF₅ on Si(001). The measured T_c is much lower than that of bulk NbC (12 K) due to the high level of impurities. The critical temperature could be increased up to 3.8 K when NH₃ was inserted in each ALD cycle following NbF₅ using the sequence TMA–NbF₅–NH₃. A transition temperature $T_c = 2.5$ K was observed when the sequence NH₃–NbF₅–TMA was used. Preliminary XPS analysis indicates that the higher transition temperatures observed for films grown with NH₃ can be attributed to the combined effect of lower fluorine content resulting from the use of a second

reducing agent and the higher bulk T_c of NbN (17 K) compared to that of NbC. Furthermore, the NbN/NbC ratio depends on the pulse sequence used; films grown using the sequence TMA–NbF₅–NH₃ contain as much as twice the NbN content as those grown with the sequence NH₃–NbF₅–TMA. This is consistent with the TiN study of Juppo and co-workers, who observed that film composition and electrical properties were dependent on the precursor sequence employed.²²

CONCLUSIONS

We demonstrated the growth of superconducting NbC_x films by ALD using NbF₅ and NbCl₅ with TMA serving as both the carbon source and the reducing agent. In situ QCM measurements confirmed linear, self-saturating growth for both processes. The TMA/NbF₅ chemistry yields a high growth rate, up to 6.3 Å/cycle, which exhibits a nonlinear dependence on deposition temperature between 125 and 350 °C. The TMA/NbCl₅ process has a comparably smaller growth rate, 1.9–2.5 Å/cycle, which increases linearly with growth temperature in the range 250–350 °C. Film density and composition were observed to be growth temperature dependent for both chemistries. Varying amounts of impurities, including amorphous carbon (a-C), AlF₃, and NbF_x were found in films grown with NbF₅, whereas only carbon and NbCl_x impurities were observed in NbCl₅ samples due to the higher volatility of AlCl₃. The films are amorphous up to a thickness of approximately 60–70 nm beyond which nanocrystals ~1–5 nm in diameter form. For NbF₅ films, electrical resistivity was found to decrease by over 4 orders of magnitude over the deposition temperature range 125–350 °C due to changes in film composition. A decrease in resistivity with increasing growth temperature was observed for samples grown with NbCl₅ at 250 and 350 °C with measured values comparable to those of the NbF₅ films. SQUID magnetometry measurements revealed a superconducting transition at $T_c = 1.8$ K in a 75 nm thick film grown at 350 °C with TMA and NbF₅. The superconducting critical temperature could be increased up to 3.8 K with the additional use of NH₃ during ALD film growth. Further work on the ALD growth and characterization of niobium carbo-nitride films is ongoing.

ASSOCIATED CONTENT

S Supporting Information. Additional details and discussion of the XPS analysis as well as TEM and CBED images of TMA/NbF₅ films. This material is available free of charge via the Internet at <http://pubs.acs.org>.

AUTHOR INFORMATION

Corresponding Author

*E-mail: jklug@anl.gov.

ACKNOWLEDGMENT

This work was supported by the U.S. Department of Energy, Office of Science under contract No. DE-AC02-06CH11357 and by the American Recovery and Reinvestment Act (ARRA) through the U.S. Department of Energy, Office of High Energy Physics Department of Science. Electron microscopy was performed at the Electron Microscopy Center for Materials Research (EMCMR) at Argonne National Laboratory, a U.S.

Department of Energy Office of Science Laboratory operated under Contract No. DE-AC02-06CH11357.

REFERENCES

- (1) Toth, L. E. *Transition Metal Carbides and Nitrides; Refractory materials*; Academic Press: New York, 1971; Vol. 7.
- (2) Pierson, H. O. *Handbook of refractory carbides and nitrides: properties, characteristics, processing, and applications*; Noyes Publications: Westwood, NJ, 1996.
- (3) Brungs, A.; York, A.; Green, M. *Catal. Lett.* **1999**, *57*, 65–69.
- (4) Kaloyeros, A.; Hoffman, M.; Williams, W. S. *Thin Solid Films* **1986**, *141*, 237–250.
- (5) Pechen, E. V.; Krasnosvobodtsev, S. I.; Shabanova, N. P.; Ekimov, E. V.; Varlashkin, A. V.; Nozdrin, V. S.; Tschovrebov, A. M.; Golovashkin, A. I. *Physica C: Supercond.* **1994**, *235–240*, 2511–2512.
- (6) Spitzer, H. J. *J. Vac. Sci. Technol.* **1973**, *10*, 20.
- (7) Zoita, C. N.; Braic, L.; Kiss, A.; Braic, M. *Surf. Coat. Technol.* **2010**, *204*, 2002–2005.
- (8) Liao, M. Y.; Gotoh, Y.; Tsuji, H.; Ishikawa, J. *J. Vac. Sci. Technol. B* **2004**, *22*, L24.
- (9) Bendavid, A.; Martin, P. J.; Kinder, T. J.; Preston, E. W. *Surf. Coat. Technol.* **2003**, *163–164*, 347–352.
- (10) Duhalde, S.; Colaco, R.; Audebert, F.; Perrone, A.; Zocco, A. *Appl. Phys. A: Mater. Sci. Process.* **1999**, *69*, S569–S571.
- (11) Ritala, M.; Leskelä, M. In *Handbook of Thin Film Materials*; Nalwa, H. S., Ed.; Academic Press: San Diego, CA, 2001; Vol. 1, pp 103–159.
- (12) Proslie, T.; Ha, Y.; Zasadzinski, J.; Ciovati, G.; Kneisel, P.; Reece, C. E.; Rimmer, R. A.; Gurevich, A. V.; Cooley, L.; Wu, G.; Pellin, M. J.; Norem, J.; Elam, J. W.; Antoine, C. Z. *Proceedings of PAC09*; Vancouver, BC, Canada, 2009; TUSPFP002.
- (13) Pajot, F.; Atik, Y.; Evesque, C.; Lefranc, S.; Leriche, B.; Torre, J.-P.; Béliet, B.; Marsot, N.; Dumoulin, L.; Bergé, L.; Piat, M.; Bréelle, E.; Prêre, D.; Benoit, A.; Hoffmann, C.; Durand, T.; Camus, P.; Santos, D.; Jin, Y.; Giard, M. *J. Low Temp. Phys.* **2008**, *151*, 513–517.
- (14) Hiltunen, L.; Leskelä, M.; Mäkelä, M.; Niinistö, L.; Nykänen, E.; Soininen, P. *Thin Solid Films* **1988**, *166*, 149–154.
- (15) Proslie, T.; Klug, J. A.; Elam, J. W.; Claus, H.; Becker, N. G.; Pellin, M. J. *J. Phys. Chem. C* **2011**, *115*, 9477–9485.
- (16) Elers, K.-E.; Haukka, S. P.; Saanila, V. A.; Kaipio, S. J.; Soininen, P. J. Deposition of transition metal carbides. U.S. Patent No. 6,482,262, Nov 19, 2002.
- (17) Kim, D.; Kim, Y.; Song, Y.; Lee, B.; Kim, J.; Suh, S.; Gordon, R. *J. Electrochem. Soc.* **2003**, *150*, C740–C744.
- (18) Hoyas, A.; Whelan, C.; Schuhmacher, J.; Maex, K.; Celis, J. *Microelectron. Eng.* **2006**, *83*, 2068–2071.
- (19) Song, M.; Rhee, S. In *ECS Transactions*; Honolulu, HI, 2008; Vol. 16, pp 227–236.
- (20) Song, M.; Rhee, S. *J. Electrochem. Soc.* **2008**, *155*, H823–H828.
- (21) Hossbach, C.; Teichert, S.; Thomas, J.; Wilde, L.; Wojcik, H.; Schmidt, D.; Adolph, B.; Bertram, M.; Muhle, U.; Albert, M.; Menzel, S.; Hintze, B.; Bartha, J. *J. Electrochem. Soc.* **2009**, *156*, H852–H859.
- (22) Juppo, M.; Alén, P.; Ritala, M.; Leskelä, M. *Chem. Vap. Deposition* **2001**, *7*, 211.
- (23) Alén, P.; Juppo, M.; Ritala, M.; Sajavaara, T.; Keinonen, J.; Leskelä, M. *J. Electrochem. Soc.* **2001**, *148*, G566.
- (24) Schmidt, D.; Knaut, M.; Hossbach, C.; Albert, M.; Dussarrat, C.; Hintze, B.; Bartha, J. *J. Electrochem. Soc.* **2010**, *157*, H638–H642.
- (25) Härkönen, K.; Doczy, M.; Lang, T.; Baxter, N. E. Deposition of carbon- and transition metal-containing thin films. U.S. Patent No. 7,198,820, April 3, 2007.
- (26) Puurunen, R. L.; Lindblad, M.; Root, A.; Krause, A. O. I. *Phys. Chem. Chem. Phys.* **2001**, *3*, 1093–1102.
- (27) Yamashita, S.; Watanuki, K.; Ishii, H.; Shiba, Y.; Kitano, M.; Shirai, Y.; Sugawa, S.; Ohmi, T. *J. Electrochem. Soc.* **2011**, *158*, H93–H96.
- (28) Elam, J. W.; Groner, M. D.; George, S. M. *Rev. Sci. Instrum.* **2002**, *73*, 2981.
- (29) Bechmann, R. *Proc. IRE* **1956**, *44*, 1600–1607.
- (30) Groner, M. D.; Fabreguette, F. H.; Elam, J. W.; George, S. M. *Chem. Mater.* **2004**, *16*, 639–645.
- (31) Elers, K.-E.; Ritala, M.; Leskelä, M.; Rauhala, E. *Appl. Surf. Sci.* **1994**, *82–83*, 468–474.
- (32) Kukli, K.; Ritala, M.; Matero, R.; Leskelä, M. *J. Cryst. Growth* **2000**, *212*, 459–468.
- (33) Tersoff, J.; Tu, Y.; Grinstein, G. *Appl. Phys. Lett.* **1998**, *73*, 2328.
- (34) Fairley, N. *CasaXPS*; Casa Software, Ltd.: Teignmouth, U.K., 2009.
- (35) McGuire, G. E.; Schweitzer, G. K.; Carlson, T. A. *Inorg. Chem.* **1973**, *12*, 2450–2453.
- (36) Ramqvist, L.; Hamrin, K.; Johansson, G.; Fahlman, A.; Nordling, C. *J. Phys. Chem. Solids* **1969**, *30*, 1835–1847.
- (37) Moulder, J. F.; Stickle, W. F.; Sobol, P. E.; Bomben, K. D. *Handbook of X-ray Photoelectron Spectroscopy*; Chastain, J., Ed.; Perkin-Elmer Corp., Physical Electronics Division: Eden Prairie, MN, 1992.
- (38) Nefedov, V. I.; Buslaev, Y. A.; Kohunov, Y. V. *Zh. Neorg. Khim.* **1974**, *19*, 1166.
- (39) Darlinski, A.; Halbritter, J. *Surf. Interface Anal.* **1987**, *10*, 223–237.
- (40) Geyer-Lippmann, J.; Simon, A.; Stollmaier, F. Z. *Anorg. Allg. Chem.* **1984**, *516*, 55–66.
- (41) Kukli, K.; Aarik, J.; Aidla, A.; Forsgren, K.; Sundqvist, J.; Hårsta, A.; Uustare, T.; Mändar, H.; Kiisler, A.-A. *Chem. Mater.* **2000**, *13*, 122–128.
- (42) Mironov, V. L.; Udalov, O. G.; Gribkov, B. A.; Fraerman, A. A. *J. Appl. Phys.* **2008**, *104*, 064301.
- (43) Kaloyeros, A. E.; Eisenbraun, E. *Annu. Rev. Mater. Sci.* **2000**, *30*, 363–385.